Environment, Development and Sustainability
https://doi.org/10.1007/s10668-022-02724-6

Treatment of pesticides (chlorpyrifos and tebuconazole) and Congo red dye by the application of green synthesized palladium nanoparticles using hemicellulose obtained from *Lallemantia royleana* seed

Almas Hamid[1,2] · Sajid Rashid Ahmad[2] · Fahad Ali[3] · Mohammad S. Iqbal[4] · Rabia Nazir[5]

Received: 11 June 2022 / Accepted: 18 October 2022

Abstract
Pesticides and dyes are significant water contaminants threatening environmental quality and compromising human health. Metal nanoparticles have appeared to be efficient in treatment of various pollutants from water. The present work reports the use of green synthesized palladium nanoparticles (Pd NPs) for removal of Congo red (CR) dye and two pesticides: chlorpyrifos (CP) and tebuconazole (TB). A highly facile and environmentally friendly synthesis of Pd NPs was achieved using hemicellulose (arabinoglucan) from *Lallemantia royleana* seeds (Tukh Malanga) at mild conditions without the addition of any reducing or stabilizing agent. Different synthetic approaches were used, viz. room temperature, heating, microwave and ultrasonication. The NPs were characterized using Fourier transform infrared spectroscopy, scanning electron microscopy, energy dispersive X-ray spectroscopy, X-ray diffraction and zeta potential measurements. NPs size varied between 15 and 61 nm having dominant hexagonal structure. Zeta potential values varied between − 5 and − 18.7 mV. The synthesized NPs exhibited excellent catalytic activity for degradation of CP, TB and CR with high adsorption capacities for CP (9245–14,633 mg g^{-1}), TB (15,882–16,745 mg g^{-1}) and CR (10,265–10,400 mg g^{-1}). The results demonstrate simple synthesis of biogenic Pd NPs employing naturally occurring substances and their potential role in eco-friendly treatment of hazardous pollutants like pesticides and dyes.

Keywords Microwave · Ultrasonic · Pesticide degradation · Dye removal · Kinetics

✉ Almas Hamid
almas209@yahoo.com

[1] College of Earth and Environmental Sciences, University of the Punjab, Lahore 54600, Pakistan

[2] Kinnaird College for Women, Lahore 54600, Pakistan

[3] Government Postgraduate College, Satellite Town, Gujranwala, Pakistan

[4] Forman Christian College, Lahore 54600, Pakistan

[5] Applied Chemistry Research Centre, Pakistan Council of Scientific and Industrial Research Laboratories Complex, Ferozepur Road, Lahore, Pakistan

Published online: 10 November 2022

1 Introduction

With increasing world population and demand for food, the production of food material is being focussed to achieve high yields by protecting them from the attack of pests. To achieve this goal, indiscriminate use of pesticides is widely practised. However, these pesticides are transported into the soil and aquatic ecosystems through agriculture runoff and erosion, thereby contaminating water bodies and causing adverse impact on aquatic organisms. Most of the applied pesticides are highly toxic and threaten environmental quality and human health due to their persistence and biomagnification along the food chain.

Organophosphates (OPs) and triazole fungicides are widely used class of pesticides. Among the many pesticides, tebuconazole (TB) and chlorpyrifos (CP) are most commonly used these days (Rani & Shanker, 2018a). Chlorpyrifos (*O*,*O*-diethyl-*O*-(3,5,6-trichloro-2-pyridinyl) phosphorothioate) is a non-systemic, broad-spectrum insecticide with moderate toxicity (Huang et al., 2015; USEPA, 2000). Long-term exposure to CP affects the human nervous, circulatory and respiratory systems. Keeping in view the uncertainty that CP inflicts no harm from cumulative exposure, the United States Environmental Protection agency (USEPA) in August 2021 revoked all "tolerances" for CP (USEPA, 2022). Tebuconazole ($C_{16}H_{22}ClN_3O$; [(RS)-1-*p*-chlorophenyl-4,4-dimethyl-3-(1H-1,2,4-triazol-1-ylmethyl) pentan-3-ol]) is a systemic triazole fungicide which displays low to moderate acute toxicity depending on route of exposure. Exposure to TB is also associated with health impacts such as neurotoxicity, thyroid toxicity, genotoxicity, reproductive toxicity and hepatoxicity in aquatic organism, particularly during developmental stages. Thus, both pesticides pose adverse impacts on the environment and potential risk to humans their presence in the environment is an issue of public concern (Altenhofen et al., 2017; Chishti et al., 2013; Gebremariam et al., 2012; Karanth et al., 2004; Oliver et al., 2000; Rani & Shanker, 2018a; Wang et al., 2016).

Azo dyes are a class of hazardous materials which are extensively used in several industries and are a major source of water pollution. Congo red (3,3′-((biphenyl)-4,4′-diylbis(azo))-bis(4-amino-1-naphthalene sulphonic acid) is a water-soluble, non-biodegradable, highly toxic and carcinogenic anionic dye commonly employed as colouring agent in rubber, textile, printing, tanneries and paper industry (Pandey et al., 2007). The release of untreated effluent from such industries containing dyes is a cause of environmental pollution and presents a challenge for the environmental protection agencies (Rajesh et al., 2014).

Many methods are used to remove and degrade such organic contaminants from environmental matrices. One such technique involves use of nanomaterials such as metals and metal oxide nanoparticles, e.g. titanium oxide, silica, iron, copper, zinc, etc. (Calza et al., 2002; Lopes et al., 2008; Polshettiwar et al., 2009; Rani & Shanker, 2018b; Stamatis et al., 2015). Palladium nanoparticles (Pd NPs) are of considerable interest due to their remarkable optical and electronic properties as well as chemical and thermal stabilities (Chen & Ostrom, 2015). Pd NPs use in homogeneous and heterogeneous catalytic reactions is well documented such as organic synthesis reactions (Astruc, 2007; Faria et al., 2014; Karimi & Enders, 2006; Lebaschi et al., 2017; Semagina et al., 2007; Tahir et al., 2016; Wilson et al., 2006; Yu et al., 2017), in catalytic convertor in vehicles, water treatment, optical sensing, hydrogen storage and sensors (Antolini, 2009; Chaudhary et al., 2018; Cookson, 2012; Martins et al., 2017). Recently, these have also gained attention as promising tools in biomedical applications and cancer therapy exhibiting appreciable anticancer and antioxidant activities (Azizi et al., 2017; Bharathiraja et al., 2018; Fahmy et al., 2020; Gil et al.,

2018; Saldan et al., 2015). The NPs either in pure or combination with other metals have also been used extensively in wastewater treatment for removal of multiple contaminants like pharmaceutical compounds (Martins et al., 2017), dyes (Li et al., 2015) and chlorinated compounds (Gautam & Suresh, 2007; Zhang et al., 2013).

Though several chemical approaches are available for synthesis of metal nanoparticles (MNPs), these involve use of variety of hazardous chemicals as reducing and capping agents and subsequent release of waste by-products into the environment. Increasing concerns over the state of present environment demand the development of eco-friendly chemical processes and products that minimize pollution and encourage cleaner production (Polshettiwar et al., 2009, 2011). In this regard, the biogenic-mediated synthesis has gained importance which exploits plant-based sources (Kalaiselvi et al., 2015; Shaik et al., 2017; Tahir et al., 2016), seaweeds (Yazdani et al., 2018) and microorganisms such as algae (Momeni & Nabipour, 2015) and bacteria (Riddin et al., 2010; Zhang et al., 2022).

A relatively recent improvement is the use of natural compounds such as hemicelluloses (polysaccharides) derived from food material. The approach offers a cost-effective and environmentally benign production of MNPs while offering many advantages over synthetic polymers by playing dual role as non-toxic and biodegradable stabilizing as well as reducing agents (Virkutyte & Varma, 2011). Being safe and eco-friendly, polysaccharides are regarded as potential hosts for synthesis of metallic NPs and have been reported to use for some noble MNPs as well (Guo et al., 2019; Huang & Yang, 2004). These can effectively coordinate with metal ions and bring about reduction and subsequent stabilization of resultant NPs, predominantly owing to presence of abundant functional groups such as hydroxyl (–OH) and carbonyl (–CO–) (Emam & Ahmed, 2016; Huang & Yang, 2004). Moreover, they are reported to form films that effectively prevent agglomeration of NPs, thereby imparting increased stability and helping in storing NPs for longer periods of time (Shah et al., 2015).

Limited studies are available for the synthesis of Pd NPs using natural polysaccharides (Guo et al., 2019; Kora & Rastogi, 2016). *Lallemantia royleana* is an important native medicinal plant, widely available in Pakistan, Afghanistan and Iran. Its seeds, commonly known as Tukh Malanga (TM) or "tukhm-e-balango," when soaked in water, swell and release mucilage (polysaccharide) which contains monosaccharides arabinose, galactose, rhamnose, xylose and glucose (Massey et al., 2016; Razavi, 2019; Salehi et al., 2018).

The present study focussed on synthesis of Pd NPs using polysaccharides from TM seeds and studied their potential for degradation of two major class of pollutants: dyes (Congo red) and pesticides (Chlorpyrifos and tebuconazole). The current research is aimed to expand avenues for polysaccharide use and will assist to reduce and manage the environmental issues which ultimately will help mitigate the environmental and health hazards associated with toxic chemicals synthesis especially NPs and environmental pollutants (pesticides and dyes). Herein we report the degradation of the above-mentioned contaminants by using green synthesized Pd nanoparticles.

2 Materials and methods

2.1 Chemicals and materials

Analytical-grade reagents and Nanopure® water were used throughout the study. Palladium chloride, hydrochloric acid and acetonitrile (HPLC grade) were procured from E

Merck, Germany. Congo red dye was purchased from Sigma-Aldrich. Chlorpyrifos and tebuconazole were supplied by local industry which is traced back to A2A Certified reference materials to confirm their purity. The neutral arabinoglucan from TM seeds, available from our laboratory from previous work, having molar mass 3.5×10^6 Da (Dalton) and comprised mainly glucose, arabinose, rhamnose (63.90, 16.39, 10.97%, respectively) and minor amounts of galactose (7.55%) and xylose (1.19%); moisture $13.67 \pm 1.7\%$ (Massey et al., 2016).

2.2 Synthesis of Pd NPs

Stock solution of $PdCl_2$ (1 mM) was prepared by dissolving 0.177 g of salt, in few drops of dilute acid (0.1 M), and making up the volume to 1000 mL. To 20 mL of $PdCl_2$ solution, varying amounts (2, 5, 10, 15 mL) of 1% polysaccharide were added under vigorous stirring to optimize the amount of polysaccharide. The pH of the mixtures after addition of the metal salts was 3.2. The total volume of the mixture was made up to 50 mL by adding deionized water. Four different set of synthetic protocols were used for synthesis of Pd NPs, i.e. (1) room temperature with simple stirring for 2 h (RT); (2) heating (70 °C) with simple stirring for 1 h (H); (3) ultrasonic synthesis for 1 h (US) and (4) microwave synthesis for 3 min at medium heat (MW). All the reactions resulted in colour change of the solution from light yellow to deep brown indicating formation of Pd NPs. The progress of Pd reduction was monitored visually and spectrophotometrically to confirm the formation of Pd NPs at regular intervals from 60 to 120 min. The synthesized Pd NPs obtained from different sets are labelled as shown in Table 1.

2.3 Characterization of palladium nanoparticles

The Pd NPs were characterized using Fourier transform infrared spectroscopy (FT-IR), scanning electron microscopy (SEM), powder X-ray diffraction (pXRD) and zeta potential measurements. FT-IR was carried out to identify the functional groups in Pd NPs and was recorded in the range of 4000–800 cm^{-1} by using ATR (Cary 630 FT-IR- Agilent Technologies). UV–Vis spectrophotometric spectra/surface plasmon resonance (SPR) spectra of Pd-TM suspension were acquired in the range of 250–800 nm using UV–Vis spectrophotometer (Shimadzu, Japan) with a scan rate of 60 nm/min with quartz cuvette cells with a 1 cm path length and TM suspension in Nanopure® water, without NPs, was taken as reference. Zetasizer Nano ZSP (Malvern, UK) was employed for hydrodynamic particle size and zeta potential (ζ) measurements using Pd-TM suspension diluted in water as per standard operating procedure of the instrument. These measurements were taken as 10 replicates, and average values were reported. The pXRD spectra were recorded by D2-Phaser (Bruker, Germany) using monochromatic Cu-Kα radiation ($\lambda = 1.5406$ Å) operating at 40 kV and 30 mA. The data were collected in the range $20° \leq 2\theta \leq 90°$. For the determination of surface morphology of Pd NPs, a SEM (Nova NanoSEM 450) equipped with an energy-dispersive X-ray spectroscopy (EDX) instrument was used and images were recorded at an accelerating voltage of 20 kV.

Table 1 Coding of Pd nanoparticles obtained by using different synthetic protocols and TM concentration

Code	Pd (1 mM) volume (mL)	TM (1%) volume (mL)	Reaction condition
TM-Pd-RT-2	20	2	Room temperature with simple stirring
TM-Pd-RT-5	20	5	
TM-Pd-RT-10	20	10	
TM-Pd-RT-15	20	15	
TM-Pd-H-2	20	2	Heating at 70 °C with simple stirring
TM-Pd-H-5	20	5	
TM-Pd-H-10	20	10	
TM-Pd-H-15	20	15	
TM-Pd-US-2	20	2	Ultrasonic
TM-Pd-US-5	20	5	
TM-Pd-US-10	20	10	
TM-Pd-US-15	20	15	
TM-Pd-MW-2	20	2	Microwave
TM-Pd-MW-5	20	5	
TM-Pd-MW-10	20	10	
TM-Pd-MW-15	20	15	

2.4 Removal of pesticides by Pd NPs

Simple experimental conditions were employed to study the pesticides removal from water at room temperature under visible light (LED light) by variation in stirring/contact time keeping pesticide concentration and Pd NPs dosage constant. The progress of the reaction was monitored by HPLC–UV. Pesticide solutions (200 mg L^{-1}) were prepared by dissolving 0.2 g of respective pesticide in 1–3 mL of acetonitrile and making up the volume up to mark with distilled water in 1000-mL volumetric flask. For pesticide removal studies, 10 mL of pesticide solution (200 mg L^{-1}) was taken in a small round-bottomed flask to which 3 mL of Pd NPs suspension was added. The reaction contents were stirred at room temperature for different time intervals (2–60 min) followed by their filtration using 0.25µ syringe filter to separate the Pd embedded in polysaccharide molecules. The resulting filtrate was subjected to HPLC-DAD (Agilent 1260, Quaternary Gradient System) to determine the residual concentration of pesticides in solution. For HPLC, 5 µL sample was injected and data were acquired by running sample on XDB-C18 5 µm, 4.6*150 mm column using acetonitrile (80):water (20) as mobile phase while keeping flow rate of 1 mL/min and column oven temperature at 24 °C. The peaks of relevant pesticides were confirmed by using A2A Certified reference standards.

The removal of pesticides proceeds through the adsorption followed by catalytic degradation. Hence, removal efficiency of NPs was determined by calculating adsorption capacity (mg g^{-1}) and application of kinetic models by using Eqs. 1–5 (Earnest et al., 2021).

$$\text{Adsorption capacity (mg g}^{-1}) \quad q_{e,exp} = \frac{(C_0 - C_e)V}{W} \tag{1}$$

$$\text{Nonlinear Chi-square} \quad \chi^2 = \sum \frac{(q_{e,exp} - q_{e,cal})^2}{q_{e,cal}^2} \tag{2}$$

Kinetic models (nonlinear)

$$\text{General order} \quad q_t = q_e - \frac{q_e}{\left[k_N (q_e)^{n-1} \times t \times (n-1) + 1\right]^{1/1-n}} \tag{3}$$

$$\text{Pseudo first order} \quad \log(q_e - q_t) = \log q_e - \frac{k_1}{2.303} t \tag{4}$$

$$\text{Pseudo second order} \quad \left(\frac{t}{q_t}\right) = \frac{1}{k_2 q_e^2} + \frac{1}{q_e} t \tag{5}$$

C_0 (mg L^{-1}), initial adsorbate concentration; C_t (mg L^{-1}), adsorbate concentrations at time t; C_e (mg L^{-1}), adsorbate concentrations at equilibrium; V (L), volume of the solution; W (g), weight of the adsorbent used.

$q_{e,exp}$ (mg g^{-1}) = experimental equilibrium capacity; $q_{e,cal}$ (mg g^{-1}) = theoretical equilibrium capacity; q_e (mg g^{-1}) = amount of adsorbent at equilibrium; q_t (mg g^{-1}) = amount of adsorbent at time t (min); k_N (min^{-1} (g $mg^{-1})^{n-1}$) = rate constants for general order; k_2 (g mg^{-1} min^{-1}) = rate constant for pseudo-second order.

2.5 Dye removal studies

The Pd NPs were tested for assessing their potential for removal of azo dyes by using Congo red (CR) dye as test contaminant. For the purpose, studies were carried out by varying contact time. The experiments were carried out by allowing 25 mL of 50 ppm dye solution to remain in contact with nanoparticles solution (2 mL). The residual concentration of the dyes was determined by acquiring absorbance data at 498 nm (Zare et al., 2015) and calculating the adsorption capacity by using Eq. 1.

3 Results and discussion

3.1 Synthesis and characterization of Pd NPs using TM

In the present work, we report a very simple and highly facile method to prepare Pd nanoparticles with TM polymer at mild conditions without the addition of any reducing or stabilizing agent. The arabinoglucan used in this study has the advantage of easily solubilizing in the water with added advantage of high yield extractability. The polymer exhibits a branched structure which facilitates the stabilization of NPs and ensures the formation of colloidal state NPs with no apparent sedimentation. Earlier studies have reported the presence of reducing sugars in the arabinoglucan which can reduce the metal salts to MNPs (Mucalo et al., 2002). The methods used are in agreement with the spirit of green

chemistry as reactions were carried out in water at mild conditions with non-hazardous hemicellulose derived from abundantly available feedstock.

3.1.1 SPR spectra of TM and Pd NPs

The SPR spectra of the 1% aqueous solution of light yellowish brown TM polysaccharide (Fig. 1) showed no characteristic absorption in the UV spectra range 200–800 nm, indicating that none of the suspensions contained any protein or acidic group. It also implied the purity of all TM polysaccharide (TM-P) aqueous suspensions.

The SPR of the all the prepared NPs was acquired over the range of 200-800 nm. The spectra hence obtained are presented in Fig. 1. In case of $PdCl_2$ the peak around 420 nm is exhibited due to absorption of Pd (II) (Schiavo et al., 2016; Shaik et al., 2017). For RT studies, the resultant solution colour is characterized by change in colour from pale yellow to deep brown indicating reduction of Pd (II) to Pd (0). In addition to change in colour, the SPR spectrum is characterized with the decrease in the intensity of $PdCl_2$ peak as the volume of TM is enhanced from 2 to 15 mL. The peak consequently disappeared at 10 mL TM indicating complete conversion of Pd (II) to Pd (0). Similar observation is recorded in rest of the three sets of reaction, i.e. H, US and MW, except that complete disappearance of the peak is observed at 15 mL TM concentration in case of US and MW. The SPR spectra of Pd NPs are characterized by a broad continuous absorption band with no SPR peak which is in line with previous studies (Schiavo et al., 2016; Shaik et al., 2017). This continuous spectrum is linked with the formation of Pd NPs having size < 10 nm (Kora & Rastogi, 2016, 2018). In case of RT and H, the highest intensity of the spectra is recorded for 10 mL TM concentration while for US and MW, 15 mL TM is considered optimized; hence, further studies were carried out at these conditions for the respective sets.

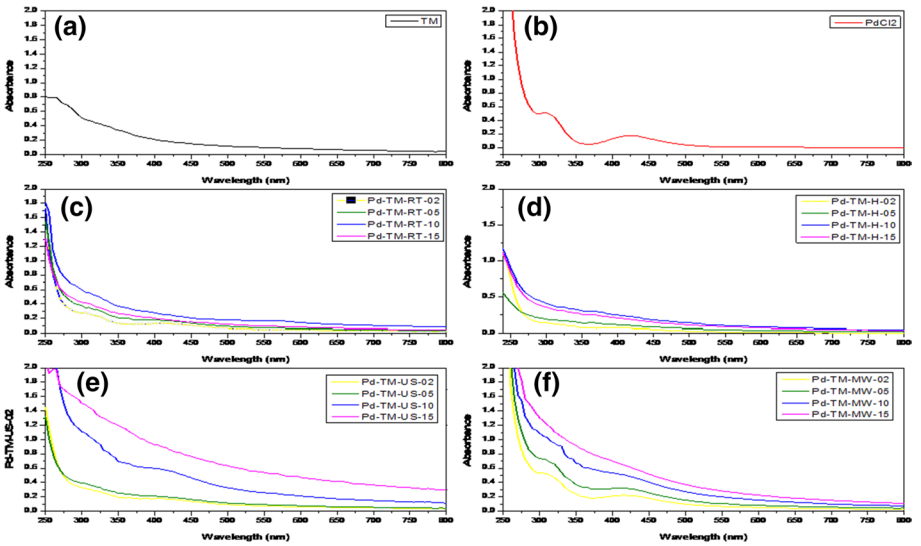

Fig. 1 UV–Vis spectroscopic study of **a** TM gel, **b** $PdCl_2$ and Pd NPs prepared **c** at room temperature, **d** heating at 70 °C **e** ultrasonic and **f** microwave

3.1.2 FT-IR analysis of TM and Pd NPs

The FT-IR spectrum of pure hemicellulose dried film is presented in Fig. 2a which is characterized by broadband at 3289 cm^{-1}: characteristic of –OH present in the polymer. The peak appearing at 2900 and 2100 cm^{-1} can be ascribed to CH stretching and bending, respectively. The peak recorded at 1709 cm^{-1} is attributed to C=O, 1599 cm^{-1} was assigned to symmetrical stretch of carboxylate group while C–H bending vibration results in peak at 1410 cm^{-1}. The small shoulder appearing at 1067 cm^{-1} and 1030 cm^{-1} point to C–O stretch of carboxylic acids. The polymer backbone bending is designated by peaks appearing below 1000 cm^{-1} (Hong et al., 2021; Iqbal et al., 2011; Kora & Rastogi, 2016).

The FT-IR spectra of optimized set of samples here by referred as TM-Pd-RT, TM-Pd-H, TM-Pd-US and TM-Pd-MW is presented in Fig. 2. Characteristics band appearing in the spectra are assigned, in comparison with analogous material reported in the literature (Kora & Rastogi, 2016; Schiavo et al., 2016; Shaik et al., 2017), as follows:

TM-Pd-RT (cm^{-1}): 3345 (OH stretching), 2929 (aliphatic saturated CH stretching), 2163 (CH bending), 1756 (C=O), 1656 (symmetrical stretch of carboxylate group), 1414 (C–H bending), 1220 (C–O stretch of carboxylic acids), 1030 (C–O stretching vibrations).

TM-Pd-H (cm^{-1}): 3330 (OH stretching), 2931 (aliphatic saturated CH stretching), 2165 (CH bending), 1722 (C=O), 1650 (symmetrical stretch of carboxylate group), 1414 (C–H bending), 1222 (C–O stretch of carboxylic acids), 1030 (C–O stretching vibrations).

TM-Pd-US (cm^{-1}): 3500 (OH stretching), 2160 (CH bending), 1649 (symmetrical stretch of carboxylate group), 1418 (C–H bending), 1149 (C–O stretch of carboxylic acids), 1032 (C–O stretching vibrations).

TM-Pd-MW (cm^{-1}): 3198 (OH stretching), 2929 (aliphatic saturated CH stretching), 2165 (CH bending), 1733 (C=O), 1638 (symmetrical stretch of carboxylate group), 1408 (C–H bending), 1224 (C–O stretch of carboxylic acids), 1034 (C–O stretching vibrations).

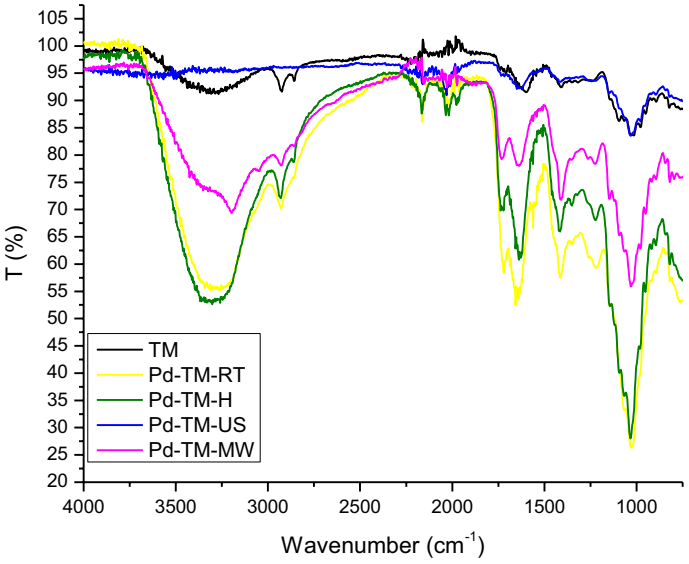

Fig. 2 FT-IR spectra of TM gel (TM) and Pd NPs prepared at room temperature (Pd-TM-RT), heating (Pd-TM-H), ultrasonication (Pd-TM-US) and microwave (Pd-TM-MW)

The spectra of all the samples depict characteristics peaks of TM (as discussed earlier) with slight shifting in frequencies of functional groups and their intensities owing to possible interaction among the functional groups and MNPs. This can be due to stabilization and possible involvement of groups like O–H and C–O in reduction of Pd (II) to Pd (0). However, no new bands indicating any Pd–polymer interaction were observed in TM-Pd NPs.

The FT-IR spectra of US and MW samples showed some changes when compared to TM like in case of –OH broad peak around 3500–3300 cm^{-1}; instead, broad peak small hump is noticed in case of US while in case of MW, unusual broadening is observed that almost overlapped the CH peaks appearing in the region of 2900 cm^{-1}. Furthermore, disappearance of C=O peak around 1700 cm^{-1} is also noticed in case of US. This can be attributed to changes in the polysaccharide structure owing to high energy reactions or their involvement in the reduction of palladium ions (Kora & Rastogi, 2016).

3.1.3 Surface morphology of Pd NPs by scanning electron microscopy

The SEM micrographs of TM solutions (Fig. 3) (Massey et al., 2016) and samples, i.e. TM-Pd-RT, TM-Pd-H, TM-Pd-US and TM-Pd-MW, were acquired at different magnifications. The average sizes of the NPs as obtained are presented in Table 2. The nanoparticles obtained from RT studies are smaller in size with less standard deviation as compared to the rest of techniques while highest size is obtained in case of US. The confirmation of the presence of Pd is done by EDX analysis, taken of the representative sample from the lot of different samples prepared, i.e. TM-Pd-RT. The EDX spectra showed the presence of Pd (1.82%) in the prepared sample. The presence of Al and Mg owed to the Al–Mg stub on which sample is mounted for acquiring data.

Difference in the morphology of TM polymer (Fig. 3a) and the one doped with Pd NPs is obvious, TM polymer has smooth morphology (as also observed in our previous studies, (Massey et al., 2016)) but incorporation of Pd into the gel structure resulted in development

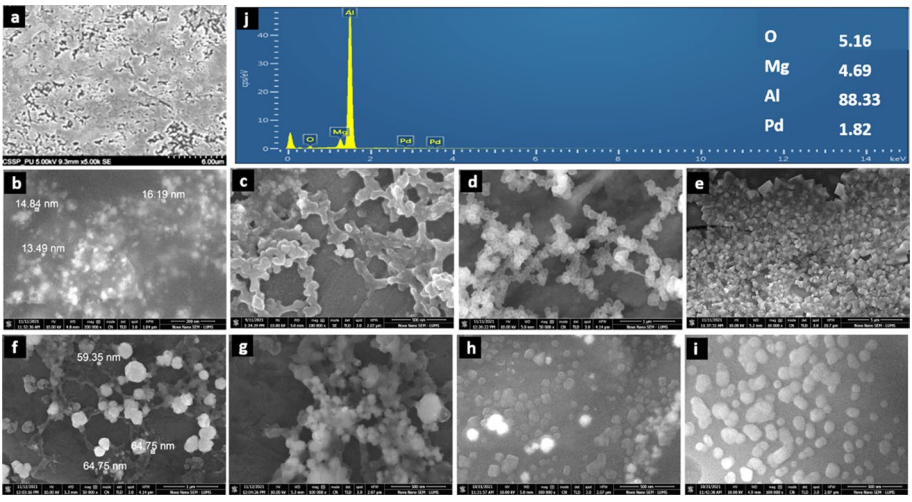

Fig. 3 SEM images of TM (**a**), Pd-TM-RT (**b**, **c**) Pd-TM-H (**d**, **e**), Pd-TM-US (**f**, **g**), Pd-TM-MW (**h**, **i**) at different resolutions and EDX image of representative sample of Pd-TM-RT (**j**)

Table 2 Physical attributes of prepared Pd NPs after 48 h (Pd-TM-RT, Pd-TM-H, Pd-TM-US, Pd-TM-MW) and after 7 months (Pd-TM-US*, Pd-TM-MW*)

Sample code	PS-SEM (nm)	PS-DLS (nm)	ZP (mV)	PDI	Conductivity (mS/cm)
TM-Pd-RT	15.2 ± 4.3	205.8	− 15.1	0.417	0.448
TM-Pd-H	56.3 ± 11.56	201.8	− 18.7	0.622	1.23
TM-Pd-US	61.7 ± 13.15	257.8	− 7.63	0.288	0.997
TM-Pd-MW	51.5 ± 13.81	386.9	− 5.02	0.469	1.26
TM-Pd-US*	–	846	− 12.3	0.652	2.11
TM-Pd-MW*	–	235	− 12.2	0.462	0.184

of buds which suggests stabilization of NPs in the gel matrix. The SEM micrograph of TM-Pd-RT (Fig. 3b, c) revealed regularly dispersed Pd NPs in polymer matrix. In case of TM-Pd-H, the particles achieved are of relatively larger size in comparison with TM-Pd-RT owing to possible change in the polysaccharide structure at higher temperatures as can be seen from the swelled buds and light threads appearing (Fig. 3d, e). The impact of high energy reactions on the gel structure is also obvious in the SEM images acquired for TM-Pd-US whereby the small buds have increased in size with more tails/threads (Fig. 3f, g). In case of TM-Pd-MW (Fig. 3h, i), there are just spongy buds available with no threads, showing that MW can affect the polysaccharide structure to greater extent as compared to simple heating and US. This is also in line with the FT-IR studies as discussed earlier.

It is also a well-established fact that size and shape of NPs are highly dependent on a number of factors such as concentration of reactants, temperature, concentration of precursors and stirring time. At room temperature, the reaction proceeds slowly so rate of formation of NPs is slow which results in smaller-sized particles. Moreover, voids in the polymer network also assist in nucleation of the NPs and provide a controlled environment (Salgueiro et al., 2013). At higher temperatures, there is more tendency of NPs aggregation due to increased kinetic energy of particles. Besides, higher temperatures may bring about changes in the polymer structure.

3.1.4 Hydrodynamic size and zeta potential measurements of Pd NPs

Hydrodynamic diameter (PS-DSL), zeta potential (ZP) and polydispersity index (PDI) of the NPs as obtained by DLS measurements are presented in Fig. 4 and listed in Table 2.

The surface charge of the Pd NPs synthesized using different methods, as measured by help of ZP, was found to be negative varying between − 5.02 and − 18.7 mV. This indicates that Pd NPs obtained from all the four techniques used are negatively charged, indicating their stability. Furthermore, negative ZP values also signify the possible capping of Pd NPs by biomolecules/polysaccharide. This negative potential will also help in preventing aggregation of NPs by yielding repulsion among the NPs (Duan et al., 2015; Xiong et al., 2020). The ZP of TM-Pd-RT particles is − 15.1 mV which is similar to the previously reported values (Abbas et al., 2019). The magnitude of NPs, however, obtained in current study was comparatively greater than reported by earlier studies (ZP 8.4 ± 1.6 mV; ZS 75.3 ± 6.7 nm) performed on Pd NPs synthesized via gum olibanum (Kora & Rastogi, 2016) while closer results were achieved when compared with Pd NPs

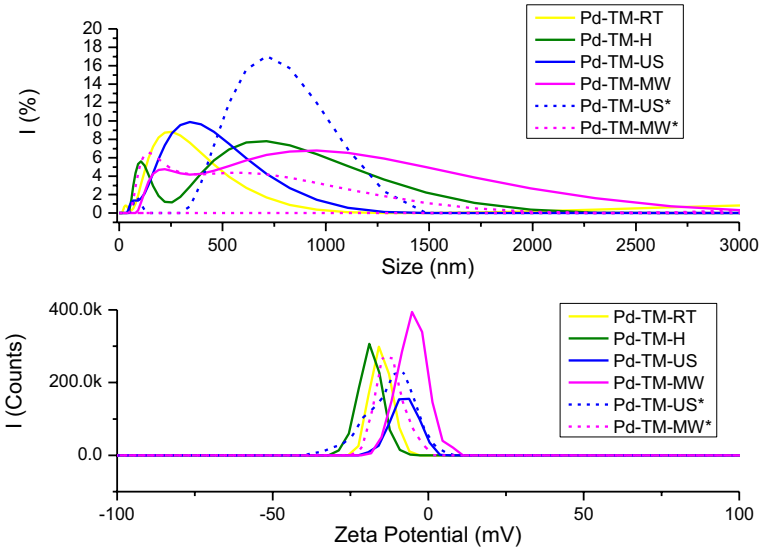

Fig. 4 Hydrodynamic size and zeta potential of Pd NPs as obtained by Dynamic light scattering studies after 48 h (Pd-TM-RT, Pd-TM-H, Pd-TM-US, Pd-TM-MW) and after 7 months (Pd-TM-US*, Pd-TM-MW*)

prepared vis arabinogalactan gum, i.e. ZP − 4.49 mV and ZS 263.4 nm (Kora, 2019; Maskos & Stauber, 2011).

Hydrodynamic size of Pd NPs obtained is larger than that obtained by SEM owing to embedding of Pd NP in the gel matrix and coating of NPs by polymer as also obvious from SEM images (Maskos & Stauber, 2011). The hydrodynamic size is an indicator of particle behaviour in a fluid. The size measured by DLS technique is not only influenced by the metallic core of MNPs but also takes into account the material adsorbed on the MNPs. Hence, for particles stabilized by polymer/surfactants, the hydrodynamic size is always larger than measured by SEM (Tomaszewska et al., 2013). Distortion of the gel structure in case of TM-Pd-MW leads to dispersion in particle size resulting to very broad curve (Fig. 4).

DLS is a reliable tool for determination of particle size distributions in terms of PDI values. The maximum value of PDI is 1 which shows broad size distribution in sample which may contain large particles (Cascio et al., 2014). Homogeneity of the prepared NPs, as indicated by PDI values, for all the samples falls below 0.7. Generally, highly mono disperse samples with narrow size distribution show values smaller than 0.1 while values bigger than 0.7 indicate a very broad particle size distribution (Danaei et al., 2018). The lower the PDI value, the narrower the size distribution and good dispersion. In the present study, the values obtained are in the range of 0.29–0.62 which may refer to moderately monodisperse nature of samples. Such small variation in the PDI of Pd NPs obtained from four different techniques also affirms the stability of NPs and less impact of reaction conditions on the particles (Emam, 2019).

3.1.5 Crystallinity of synthesized Pd NPs

The XRD spectra of Pd NPs (Pd-TM-RT-10, Pd-TM-H-10, Pd-TM-US-15, Pd-TM-US-15) are presented in Fig. 5. The XRD spectra of Pd-TM-RT-10 and Pd-TM-H-10 are showing amorphous nature of sample with no characteristic peaks. Such kind of spectra is typical of small-sized NPs which is in line with previous studies (Schiavo et al., 2016). In case of Pd-TM-MW and Pd-TM-US, the XRD pattern is characterized by peaks appearing at 2θ values of 36.3, 40.3, 42.5, 46.5, 66.2 and 36.3, 40.5, 46.8 and 66.5, respectively, which corresponds to diffraction peaks of 100 referring to hexagonal palladium and 200, 020, 220 referring to fcc palladium. The high intensity of the Pd hexagonal peak, i.e. 100, refers to being prominent phase.

3.2 Contaminants removal with Pd NPs

The Pd NPs catalytic performance was assessed by selecting two pesticides (Chlorpyrifos, CP and tebuconazole, TB) and a dye (Congo red, CR) as test contaminants.

3.2.1 Removal studies of dye

Room temperature dye (Congo red, CR) degradation studies were carried out for all the four samples (Pd-TM-RT, Pd-TM-H, Pd-TM-US, Pd-TM-MW) by varying contact time (2–60 min). The percentage degradation of dye was studied by analysing the residual concentration of dye after treatment using spectrophotometer. It was observed that with increase in the contact time percentage removal of CR increases resulting in optimized time at 30 min in all the four cases (Fig. 6). High adsorption capacity

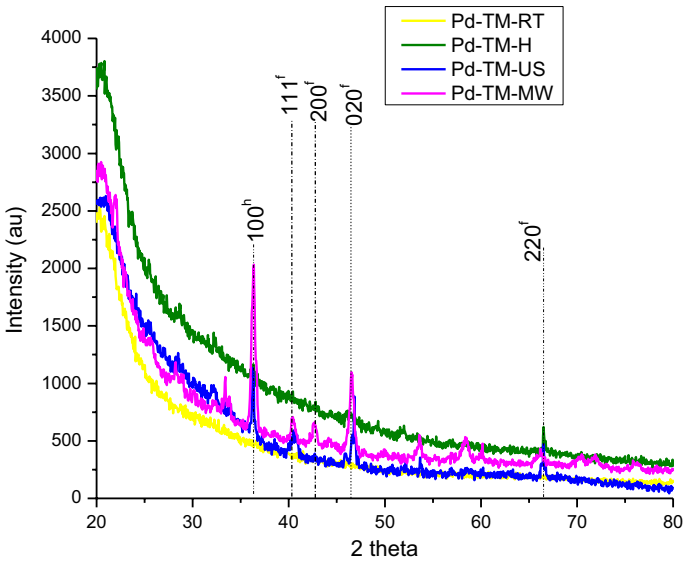

Fig. 5 XRD diffractogram of prepared Pd Nanoparticles JCPDS file no 72-0710 (hexagonal) and JCPDS file no. 87–0638 (fcc)

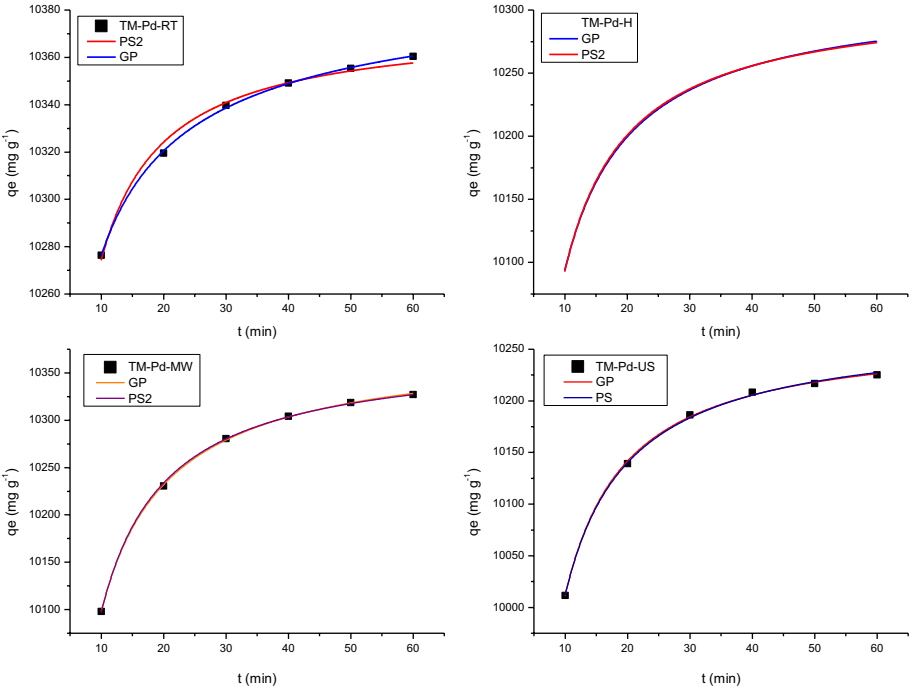

Fig. 6 Effect of contact time on degradation of CR (■) by palladium nanoparticles and fitting of kinetic models

is observed which follows the order: TM-Pd-RT (10,400.0 mg g^{-1}) > TM-Pd-MW (10,383.2 mg g^{-1}) > TM-Pd-H (10,318.2 mg g^{-1}) > TM-Pd-US (10,265.0 mg g^{-1}). The enhanced activity of Pd NPs can be attributed to adsorption capacity because of the porosity of TM polymer which is due to its heterogeneity and highly branched structure. Pd is known for its high activity which is considerably enhanced with reduction in particle size. Further the presence of polysaccharide also favours the adsorption and then degradation of contaminants. Earlier, acacia gum-mediated Pd NPs were reported to drastically increase the rate of dye degradation (Emam et al., 2020).

In the present study, 80% dye removal was achieved as compared to removal (23%) by Pd catalyst based on chitosan–tannin framework (Bhat et al., 2019), whereas 95.32% reduction of CR was reported by (Pd NPs) synthesized using agro-waste empty cotton boll peels aqueous extract (Narasaiah & Mandal, 2020). Moreover, silver (Ag) nanoparticles, synthesized and stabilized by exo polysaccharide, have also shown good CR removal efficiency (Saravanan et al., 2017). However, the current studies have added advantage of undergoing high degradation of CR by using Pd NPs alone which is in contrast to earlier studies on CR degradation that reported the use of sodium borohydride as an additive for facilitating the mineralization of the dye (Malik et al., 2021; Narasaiah & Mandal, 2020) which is itself a strong reducing agent. Moreover, the amount of Pd NPs used in the present study is far less than reported earlier.

Three kinetic models were chosen out of which general pseudo-order (GP) fits well in all the four cases while pseudo-first kinetic (PF) did not converge well; hence, the fitting and parameters related to it are not presented in Fig. 6 and Table 3.

Table 3 Adsorption kinetics fitting parameters for pesticides (CP and TB) and dye (CR) adsorption on Pd NPs (Pd-TM-RT, Pd-TM-H, Pd-TM-US, Pd-TM-MW) along with the goodness of fit parameters

Model	Parameter	Pd-TM-RT			Pd-TM-H			Pd-TM-US			Pd-TM-MW		
		CP	TB	CR	CP	TB	CR	CP	TB	CR	CP	TB	CR
General order	$q_{e,exp}$ (mg g^{-1})	10,887.1	15,010.2	10,339.7	13,850	14,629	10,238.5	11,994.4	14,517	10,186.4	8798.6	13,443.5	10,280.6
	k (min^{-1})	6.0e−5	1.47e−4	3.38e−5	2.8e−5	7.2e−5	2.7e−4	3.8e−5	0.016	5.7e−4	0.029	1.7e−5	2.08e−4
	$q_{e,cal}$ (mg g^{-1})	14,633.8	16,600.9	10,400.0	11,644.6	16,745.2	10,318.2	12,577.4	15,882.3	10,265.0	9245.0	16,410.5	10,383.2
	R_{adj}^2	0.9999	0.9999	0.9992	0.9999	0.9999	0.9994	0.9998	0.9999	0.9989	0.9999	0.9999	0.997
	SD	2.06	4.87	0.88	2.11	7.99	1.62	9.38	10.02	2.65	7.49	10.17	1.57
	Reduced-χ^2	4.26	23.69	0.78	4.47	63.96	2.64	88.09	100.51	7.05	56.22	103.39	2.46
Pseudo-second order	k_2 (min^{-1})	2.6e−5	8.9e−5	9.8e−4	3.1e−5	6.8e−5	4.5e−4	4.1e−5	6.9e−6	3.75e−4	1.8e−5	8.5e−6	3.5e−4
	$q_{e,cal}$ (mg g^{-1})	14,737.6	16,693.2	10,374.5	11,634.3	16,755.9	10,311.3	12,571.9	18,018.2	10,271.6	10,171.6	16,590.7	10,374.4
	R_{adj}^2	0.9998	0.9999	0.9909	0.9999	0.9999	0.9993	0.9998	0.9840	0.9989	0.9737	0.9999	0.9995
	SD	13.18	9.48	2.99	2.17	7.00	1.78	8.17	283.7	2.58	168.2	16.23	1.93
	Reduced-χ^2	173.6	89.96	8.94	4.73	49.02	3.17	66.53	80,475.6	6.64	28,293.9	263.5	3.73

3.2.2 Removal of pesticides

Room temperature visible light catalysed pesticides' adsorption/degradation studies were carried out for all the four samples (Pd-TM-RT, Pd-TM-H, Pd-TM-US, Pd-TM-MW) by varying contact time (2–60 min). The percentage adsorption/degradation of pesticides was studied by analysing the residual concentration of pesticides after treatment using HPLC-UV.

The adsorption varied with contact time and studies showed that for CP, optimized time attained to reach maximum adsorption capacity is 40 min except for Pd-TM-MW where it is 30 min. For TB, complete removal was observed at 10 min for Pd-TM-RT and Pd-TM-H as no peak appeared in HPLC chromatogram at retention time of TB. Hence, the studies were repeated for said samples by varying the time from 2 to 12 min. The studies showed that optimized time for these two cases comes out to be 6 min while for Pd-TM-MW and Pd-TM-US the optimized time is 30 min as shown in Fig. 7. High adsorption capacity is observed in all the four cases, i.e. for both the pesticides. Highest uptake/degradation potential (14,633.8; 16,745.2 mg g^{-1}) is observed in case of Pd-TM-RT for CP and Pd-TM-H for TB, respectively.

The higher uptake of pesticide and dye on Pd NPs can be attributed to their small size and high porosity of the polymer as also depicted by SEM images. The porous polymer results in greater dispersion of the particles and higher stability. High surface area-to-volume ratio of NPs offers vast reactive interface between the particle and its environment.

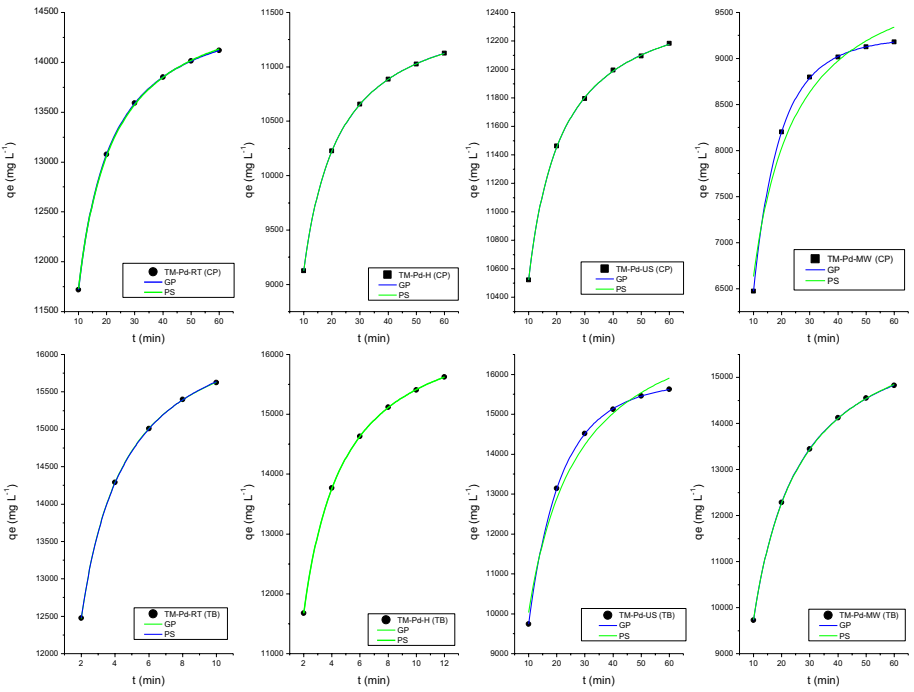

Fig. 7 Effect of contact time on degradation of CP (■) and TB (●) by palladium nanoparticles and fitting of kinetic models

For insight into the adsorption process, three kinetic models (general pseudo-order (GP), pseudo-first-order (PF) and pseudo-second-order kinetic (PS) were chosen out of which GP fits well in all the four cases while PF did not converge well; hence, the fitting and parameters related to it are not presented in Fig. 7 and Table 3.

The studies showed that in all the four cases, the uptake capacity for TB is higher than CP. In case of CP the order follows is: TM-Pd-RT > TM-Pd-US > TM-Pd-H > TM-Pd-MW while for TB: TM-Pd-H > TM-Pd-RT > TM-Pd-MW > TM-Pd-US. The reason of comparatively less activity of MW and US NPs can be attributed to particle size as affirmed from Table 2 as well as distorting of polymer structuring that led to less absorption of pesticides and hence degradation.

A representative CP sample after treatment was run on LC-MS-MS (Agilent) to compare the chromatogram for presence of degradation products. The spectra (Fig. 8) hence obtained were compared with standard spectra that showed single peak arising due to CP at RT of 7.565 min with basic fragmentation pattern of $m/z = 97$ and 197.8. The chromatogram of samples showed the appearance of few additional peaks, other than chlorpyrifos which points to the formation of one main degradation product with m/z value of 70 (base peak), 115.2 and 124.9.

The possible degradation mechanism involves oxidation of the organic substances due to the presence of dissolved oxygen (DO) in the Pd NPs suspensions used for treatment of

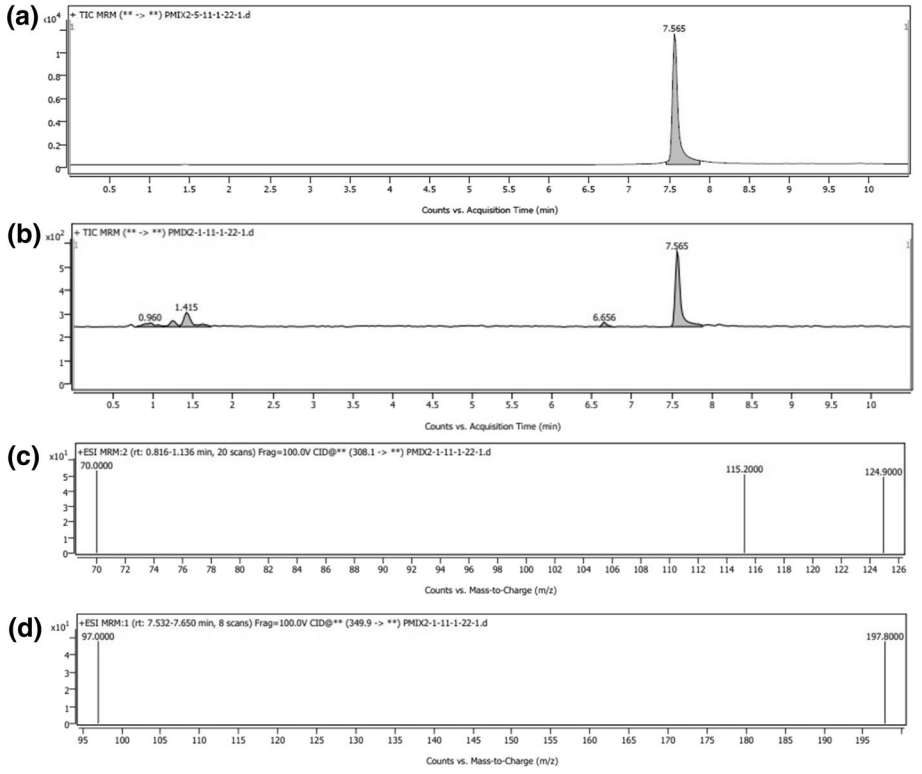

Fig. 8 Total ion chromatograms of CP standard (**a**) and representative treated sample (**b**) along with the m/z fragmentation pattern of the samples at RT of 0.960 min (**c**) and 7.565 min (**d**)

pesticides solution. The DO levels were approximately 10–11 ppm in all Pd NPs samples as measured by DO meter (Jenway, model 970). The role of Pd NPs was to drastically reduce the activation energy of the oxidation process by adsorption of pesticides on the surface of the catalyst.

Earlier, noble MNPs have been reported to facilitate halogenation of chlorocarbons. According to Nair & Pradeep (2003), complete mineralization of halocarbons was achieved at room temperature using silver (Ag) and gold (Au) NPs. Similarly, degradation of CP by Au and Ag has been reported (Bootharaju & Pradeep, 2012).

4 Conclusion

Polysaccharide-assisted Pd NPs were prepared effectively using four different synthetic approaches that include variation in amount of polysaccharide gel (2, 5, 10 and 15 mL) simple stirring at room temperature, heating with simple stirring, ultrasonication and microwave synthesis. The conversion of Pd (II) to Pd (0) is optimized at 10 mL for simple stirring and heating while it is 15 mL for ultrasonic and microwave. The average size of NPs obtained at optimized doses falls in the range of 15.2–61.7 nm (Pd-TM-RT = 15.2 ± 4.3 nm, Pd-TM-H = 56.3 ± 11.56 nm, Pd-TM-US = 61.7 ± 13.15 nm and Pd-TM-MW = 51.5 ± 13.81 nm) having dominant hexagonal structure. Smallest size is achieved at room temperature experiments with regularly dispersed Pd NPs in the well-structured gel. With the increase in the temperature and high energy reactions (US and MW), the deformation of gel becomes evident. The NPs suspension in gel solution forms a stable structure as evidenced by zeta potential values. The prepared NPs have very high degradation potential towards pesticides (chlorpyrifos and tebuconazole) and reactive dye (Congo red). In all the Pd NPs case, the highest degradation potential was achieved for CR followed by TB and CP while among the NPs, Pd-TM-RT showed highest degradation for CP (14,634 mg g^{-1}) and CR (10,400 mg g^{-1}) while Pd-TM-H showed TB (16,745 mg g^{-1}). Hence, the green synthesis protocol using either room temperature stirring or simple stirring with heating leads to improved degradation of the organic contaminants.

Funding The authors declare that no funds, grants or other support were received during the preparation of this manuscript.

Data availability The datasets generated during and/or analysed during the current study are available from the corresponding author on request.

Declarations

Conflict of interest The authors have no relevant financial or non-financial interests to disclose.

References

Abbas, G., Kumar, N., Kumar, D., & Pandey, G. (2019). Effect of reaction temperature on shape evolution of palladium nanoparticles and their cytotoxicity against A-549 lung cancer cells. *ACS Omega, 4*, 21839–21847.

Altenhofen, S., Nabinger, D. D., Wiprich, M. T., Pereira, T. C. B., Bogo, M. R., & Bonan, C. D. (2017). Tebuconazole alters morphological, behavioral and neurochemical parameters in larvae and adult zebrafish (*Danio rerio*). *Chemosphere, 180*, 483–490.

Antolini, E. (2009). Palladium in fuel cell catalysis. *Energy & Environmental Science, 2*, 915–931.
Astruc, D. (2007). Palladium nanoparticles as efficient green homogeneous and heterogeneous carbon–carbon coupling precatalysts: A unifying view. *Inorganic Chemistry, 46*, 1884–1894.
Azizi, S., Shahri, M. M., Rahman, H. S., Rahim, R. A., Rasedee, A., & Mohamad, R. (2017). Green synthesis palladium nanoparticles mediated by white tea (*Camellia sinensis*) extract with antioxidant, antibacterial, and antiproliferative activities toward the human leukemia (MOLT-4) cell line. *International Journal of Nanomedicine, 12*, 8841.
Bharathiraja, S., Bui, N. Q., Manivasagan, P., Moorthy, M. S., Mondal, S., Seo, H., Phuoc, N. T., Vy Phan, T. T., Kim, H., Lee, K. D., & Oh, J. (2018). Multimodal tumor-homing chitosan oligosaccharide-coated biocompatible palladium nanoparticles for photo-based imaging and therapy. *Scientific Reports, 8*, 1–16.
Bhat, I. U. H., Anwar, M. N. K., & Appaturi, J. N. (2019). Polymer based palladium nanocatalyst for the degradation of nitrate and Congo red. *Journal of Polymers and the Environment, 27*, 1475–1487.
Bootharaju, M., & Pradeep, T. (2012). Understanding the degradation pathway of the pesticide, chlorpyrifos by noble metal nanoparticles. *Langmuir, 28*, 2671–2679.
Calza, P., Baudino, S., Aigotti, R., Baiocchi, C., Branca, P., & Pelizzetti, E. (2002). High-performance liquid chromatographic/tandem mass spectrometric identification of the phototransformation products of tebuconazole on titanium dioxide. *Journal of Mass Spectrometry, 37*, 566–576.
Cascio, C., Gilliland, D., Fo, R., Calzolai, L., & Contado, C. (2014). Critical experimental evaluation of key methods to detect, size and quantify nanoparticulate silver. *Analytical Chemistry, 86*, 12143–12151.
Chaudhary, R. P., Barman, S. K., Huda, M. N., & Koymen, A. R. (2018). One-step hydrogen extraction and storage in plasma generated palladium nanoparticles. *Journal of Nanoparticle Research, 20*, 1–14.
Chen, A., & Ostrom, C. (2015). Palladium-based nanomaterials: Synthesis and electrochemical applications. *Chemical Reviews, 115*, 11999–12044.
Chishti, Z., Hussain, S., Arshad, K. R., Khalid, A., & Arshad, M. (2013). Microbial degradation of chlorpyrifos in liquid media and soil. *Journal of Environmental Management, 114*, 372–380.
Cookson, J. (2012). The preparation of palladium nanoparticles. *Platinum Metals Review, 56*, 83–98.
Danaei, M., Dehghankhold, M., Ataei, S., Hasanzadeh Davarani, F., Javanmard, R., Dokhani, A., Khorasani, S., & Mozafari, M. R. (2018). Impact of particle size and polydispersity index on the clinical applications of lipidic nanocarrier systems. *Pharmaceutics, 10*, 57.
Duan, L., Li, M., & Liu, H. (2015). Biosynthesised palladium nanoparticles using *Eucommia ulmoides* bark aqueous extract and their catalytic activity. *IET Nanobiotechnology, 9*, 349–354.
Earnest, I., Nazir, R., & Hamid, A. (2021). Quality assessment of drinking water of Multan city, Pakistan in context with Arsenic and Fluoride and use of Iron nanoparticle doped kitchen waste charcoal as a potential adsorbent for their combined removal. *Applied Water Science, 11*, 191. https://doi.org/10.1007/s13201-021-01531-0
Emam, H. E. (2019). Arabic gum as bio-synthesizer for Ag–Au bimetallic nanocomposite using seed-mediated growth technique and its biological efficacy. *Journal of Polymers and the Environment, 27*, 210–223.
Emam, H. E., & Ahmed, H. B. (2016). Polysaccharides templates for assembly of nanosilver. *Carbohydrate Polymers, 135*, 300–307.
Emam, H. E., Saad, N. M., Abdallah, A. E., & Ahmed, H. B. (2020). Acacia gum versus pectin in fabrication of catalytically active palladium nanoparticles for dye discoloration. *International Journal of Biological Macromolecules, 156*, 829–840.
Fahmy, S. A., Preis, E., Bakowsky, U., & Azzazy, H.M.E.-S. (2020). Palladium nanoparticles fabricated by green chemistry: Promising chemotherapeutic, antioxidant and antimicrobial agents. *Materials, 13*, 3661.
Faria, V. W., Oliveira, D. G., Kurz, M. H., Gonçalves, F. F., Scheeren, C. W., & Rosa, G. R. (2014). Palladium nanoparticles supported in a polymeric membrane: An efficient phosphine-free "green" catalyst for Suzuki-Miyaura reactions in water. *RSC Advances, 4*, 13446–13452.
Gautam, S. K., & Suresh, S. (2007). Studies on dechlorination of DDT (1,1,1-trichloro-2,2-bis(4-chlorophenyl)ethane) using magnesium/palladium bimetallic system. *Journal of Hazardous Materials, 139*, 146–153. https://doi.org/10.1016/j.jhazmat.2006.06.017
Gebremariam, S. Y., Beutel, M. W., Yonge, D. R., Flury, M., & Harsh, J. B. (2012). Adsorption and desorption of chlorpyrifos to soils and sediments. *Reviews of Environmental Contamination and Toxicology, 215*, 123–175.
Gil, Y.-G., Kang, S., Chae, A., Kim, Y.-K., Min, D.-H., & Jang, H. (2018). Synthesis of porous Pd nanoparticles by therapeutic chaga extract for highly efficient tri-modal cancer treatment. *Nanoscale, 10*, 19810–19817.

Guo, X., Zhang, J., Cui, Y., Chen, S., Sun, H., Yang, Q., Ma, G., Wang, L., & Kang, J. (2019). Highly biocompatible jujube polysaccharide-stabilized palladium nanoparticles with excellent catalytic performance. *New Journal of Chemistry, 43*, 7646–7652.

Hong, T., Yin, J.-Y., Nie, S.-P., & Xie, M.-Y. (2021). Applications of infrared spectroscopy in polysaccharide structural analysis: Progress, challenge and perspective. *Food Chemistry X, 12*, 100168. https://doi.org/10.1016/j.fochx.2021.100168

Huang, H., & Yang, X. (2004). Synthesis of polysaccharide-stabilized gold and silver nanoparticles: A green method. *Carbohydrate Research, 339*, 2627–2631.

Huang, S., Hu, J., Guo, P., Liu, M., & Wu, R. (2015). Rapid detection of chlorpyriphos residue in rice by surface-enhanced Raman scattering. *Analytical Methods, 7*, 4334–4339.

Iqbal, M. S., Akbar, J., Saghir, S., Karim, A., Koschella, A., Heinze, T., & Sher, M. (2011). Thermal studies of plant carbohydrate polymer hydrogels. *Carbohydrate Polymers, 86*, 1775–1783.

Kalaiselvi, A., Roopan, S. M., Madhumitha, G., Ramalingam, C., & Elango, G. (2015). Synthesis and characterization of palladium nanoparticles using *Catharanthus roseus* leaf extract and its application in the photo-catalytic degradation. *Spectrochimica Acta Part A: Molecular and Biomolecular Spectroscopy, 135*, 116–119. https://doi.org/10.1016/j.saa.2014.07.010

Karanth, S., Liu, J., Olivier, K., Jr., & Pope, C. (2004). Interactive toxicity of the organophosphorus insecticides chlorpyrifos and methyl parathion in adult rats. *Toxicology and Applied Pharmacology, 196*, 183–190.

Karimi, B., & Enders, D. (2006). New N-heterocyclic carbene palladium complex/ionic liquid matrix immobilized on silica: Application as recoverable catalyst for the Heck reaction. *Organic Letters, 8*, 1237–1240.

Kora, A. J. (2019). Plant arabinogalactan gum synthesized palladium nanoparticles: Characterization and properties. *Journal of Inorganic and Organometallic Polymers and Materials, 29*, 2054–2063.

Kora, A. J., & Rastogi, L. (2016). Catalytic degradation of anthropogenic dye pollutants using palladium nanoparticles synthesized by gum olibanum, a glucuronoarabinogalactan biopolymer. *Industrial Crops and Products, 81*, 1–10.

Kora, A. J., & Rastogi, L. (2018). Green synthesis of palladium nanoparticles using gum ghatti (*Anogeissus latifolia*) and its application as an antioxidant and catalyst. *Arabian Journal of Chemistry, 11*, 1097–1106.

Lebaschi, S., Hekmati, M., & Veisi, H. (2017). Green synthesis of palladium nanoparticles mediated by black tea leaves (*Camellia sinensis*) extract: Catalytic activity in the reduction of 4-nitrophenol and Suzuki-Miyaura coupling reaction under ligand-free conditions. *Journal of Colloid and Interface Science, 485*, 223–231.

Li, S., Li, H., Liu, J., Zhang, H., Yang, Y., Yang, Z., Wang, L., & Wang, B. (2015). Highly efficient degradation of organic dyes by palladium nanoparticles decorated on 2D magnetic reduced graphene oxide nanosheets. *Dalton Transactions, 44*, 9193–9199.

Lopes, R. P., de Urzedo, A. P., Nascentes, C. C., & Augusti, R. (2008). Degradation of the insecticides thiamethoxam and imidacloprid by zero-valent metals exposed to ultrasonic irradiation in water medium: Electrospray ionization mass spectrometry monitoring. *Rapid Communications in Mass Spectrometry, 22*, 3472–3480.

Malik, M. A., Alshehri, A. A., Abomuti, M. A., Danish, E. Y., & Patel, R. (2021). Bioengineered *Matricaria recutita* extract-assisted palladium nanoparticles for the Congo red dye degradation and catalytic reduction of 4-nitrophenol to 4-aminophenol. *Toxics, 9*, 103.

Martins, M., Mourato, C., Sanches, S., Noronha, J. P., Crespo, M. B., & Pereira, I. A. (2017). Biogenic platinum and palladium nanoparticles as new catalysts for the removal of pharmaceutical compounds. *Water Research, 108*, 160–168.

Maskos, M., & Stauber, R. (2011). Characterization of nanoparticles in biological environments. In P. Ducheyne (Ed.), *Comprehensive biomaterials* (pp. 329–339). Elsevier.

Massey, S., Iqbal, M. S., Wolf, B., Mariam, I., & Rao, S. (2016). Comparative drug loading and release study on some carbohydrate polymers. *Latin American Journal of Pharmacy, 35*, 146–155.

Momeni, S., & Nabipour, I. (2015). A simple green synthesis of palladium nanoparticles with Sargassum alga and their electrocatalytic activities towards hydrogen peroxide. *Applied Biochemistry and Biotechnology, 176*, 1937–1949.

Mucalo, M., Bullen, C., Manley-Harris, M., & McIntire, T. M. (2002). Arabinogalactan from the Western larch tree: A new, purified and highly water-soluble polysaccharide-based protecting agent for maintaining precious metal nanoparticles in colloidal suspension. *Journal of Materials Science, 37*, 493–504.

Nair, A. S., & Pradeep, T. (2003). Halocarbon mineralization and catalytic destruction by metal nanoparticles. *Current Science, 84*, 1560–1564.

Narasaiah, B. P., & Mandal, B. K. (2020). Remediation of azo-dyes based toxicity by agro-waste cotton boll peels mediated palladium nanoparticles. *Journal of Saudi Chemical Society, 24*, 267–281.
Oliver, G., Bolles, H., & Shurdut, B. (2000). Chlorpyrifos: Probabilistic assessment of exposure and risk. *Neurotoxicology, 21*, 203–208.
Pandey, A., Singh, P., & Iyengar, L. (2007). Bacterial decolorization and degradation of azo dyes. *International Biodeterioration & Biodegradation, 59*, 73–84.
Polshettiwar, V., Len, C., & Fihri, A. (2009). Silica-supported palladium: Sustainable catalysts for cross-coupling reactions. *Coordination Chemistry Reviews, 253*, 2599–2626.
Polshettiwar, V., Luque, R., Fihri, A., Zhu, H., Bouhrara, M., & Basset, J.-M. (2011). Magnetically recoverable nanocatalysts. *Chemical Reviews, 111*, 3036–3075.
Rajesh, R., Kumar, S. S., & Venkatesan, R. (2014). Efficient degradation of azo dyes using Ag and Au nanoparticles stabilized on graphene oxide functionalized with PAMAM dendrimers. *New Journal of Chemistry, 38*, 1551–1558.
Rani, M., & Shanker, U. (2018a). Degradation of traditional and new emerging pesticides in water by nanomaterials: Recent trends and future recommendations. *International Journal of Environmental Science and Technology, 15*, 1347–1380.
Rani, M., & Shanker, U. (2018b). Removal of chlorpyrifos, thiamethoxam, and tebuconazole from water using green synthesized metal hexacyanoferrate nanoparticles. *Environmental Science and Pollution Research, 25*, 10878–10893.
Razavi, S. M. (2019). *Emerging natural hydrocolloids: Rheology and functions*. Wiley.
Riddin, T., Gericke, M., & Whiteley, C. G. (2010). Biological synthesis of platinum nanoparticles: Effect of initial metal concentration. *Enzyme and Microbial Technology, 46*, 501–505. https://doi.org/10.1016/j.enzmictec.2010.02.006
Saldan, I., Semenyuk, Y., Marchuk, I., & Reshetnyak, O. (2015). Chemical synthesis and application of palladium nanoparticles. *Journal of Materials Science, 50*, 2337–2354.
Salehi, M., Tabarsa, M., Amraie, M., Anvari, M., Rezaei, M., & Smith, B. M. (2018). Characterization of rheological and structural properties of a gum from Balangu seeds. *International Journal of Biological Macromolecules, 117*, 294–300.
Salgueiro, A. M., Daniel-da-Silva, A. L., Fateixa, S., & Trindade, T. (2013). κ-Carrageenan hydrogel nanocomposites with release behavior mediated by morphological distinct Au nanofillers. *Carbohydrate Polymers, 91*, 100–109.
Saravanan, C., Rajesh, R., Kaviarasan, T., Muthukumar, K., Kavitake, D., & Shetty, P. H. (2017). Synthesis of silver nanoparticles using bacterial exopolysaccharide and its application for degradation of azo-dyes. *Biotechnology Reports, 15*, 33–40.
Schiavo, L., Aversa, L., Tatti, R., Verucchi, R., & Carotenuto, G. (2016). Structural characterizations of palladium clusters prepared by polyol reduction of [PdCl4] 2− ions. *Journal of Analytical Methods in Chemistry, 2016*, 1–6.
Semagina, N., Grasemann, M., Xanthopoulos, N., Renken, A., & Kiwi-Minsker, L. (2007). Structured catalyst of Pd/ZnO on sintered metal fibers for 2-methyl-3-butyn-2-ol selective hydrogenation. *Journal of Catalysis, 251*, 213–222.
Shah, U., Gani, A., Ashwar, B. A., Shah, A., Ahmad, M., Gani, A., Wani, I. A., & Masoodi, F. A. (2015). A review of the recent advances in starch as active and nanocomposite packaging films. *Cogent Food & Agriculture, 1*, 1115640.
Shaik, M. R., Ali, Z. J., Khan, M., Kuniyil, M., Assal, M. E., Alkhathlan, H. Z., Al-Warthan, A., Siddiqui, M. R., Khan, M., & Adil, S. F. (2017). Green synthesis and characterization of palladium nanoparticles using *Origanum vulgare* L. extract and their catalytic activity. *Molecules, 22*, 165.
Stamatis, N., Antonopoulou, M., & Konstantinou, I. (2015). Photocatalytic degradation kinetics and mechanisms of fungicide tebuconazole in aqueous TiO_2 suspensions. *Catalysis Today, 252*, 93–99.
Tahir, K., Nazir, S., Li, B., Ahmad, A., Nasir, T., Khan, A. U., Shah, S. A., Khan, Z. U., Yasin, G., & Hameed, M. U. (2016). Sapium sebiferum leaf extract mediated synthesis of palladium nanoparticles and in vitro investigation of their bacterial and photocatalytic activities. *Journal of Photochemistry and Photobiology B: Biology, 164*, 164–173. https://doi.org/10.1016/j.jphotobiol.2016.09.030
Tomaszewska, E., Soliwoda, K., Kadziola, K., Tkacz-Szczesna, B., Celichowski, G., Cichomski, M., Szmaja, W., & Grobelny, J. (2013). Detection limits of DLS and UV–Vis spectroscopy in characterization of polydisperse nanoparticles colloids. *Journal of Nanomaterials, 2013*, 1–10.
USEPA. (2000). *USEPA Office of prevention, pesticides and toxic substance chlorpyrifos: Revised product and residue chemistry chapters*. US Environmental Protection Agency.
USEPA. (2022). Chlorpyrifos. Environmental Protection Agency. https://www.epa.gov/ingredients-used-pesticide-products/chlorpyrifos. Accessed 16 August 2022.
USEPA Oopats. (2000b). Chlorpyriphos and registration standard.

Virkutyte, J., & Varma, R. S. (2011). Green synthesis of metal nanoparticles: Biodegradable polymers and enzymes in stabilization and surface functionalization. *Chemical Science, 2*, 837–846.

Wang, C., Wang, F., Zhang, Q., & Liang, W. (2016). Individual and combined effects of tebuconazole and carbendazim on soil microbial activity. *European Journal of Soil Biology, 72*, 6–13.

Wilson, O. M., Knecht, M. R., Garcia-Martinez, J. C., & Crooks, R. M. (2006). Effect of Pd nanoparticle size on the catalytic hydrogenation of allyl alcohol. *Journal of the American Chemical Society, 128*, 4510–4511.

Xiong, Y., Huang, L., Mahmud, S., Yang, F., & Liu, H. (2020). Bio-synthesized palladium nanoparticles using alginate for catalytic degradation of azo-dyes. *Chinese Journal of Chemical Engineering, 28*, 1334–1343. https://doi.org/10.1016/j.cjche.2020.02.014

Yazdani, A., Sayadi, M., & Heidari, A. (2018). Green biosynthesis of palladium oxide nanoparticles using dictyota indica seaweed and its application for adsorption. *Journal of Water and Environmental Nanotechnology, 3*, 337–347.

Yu, D., Bai, J., Wang, J., Liang, H., & Li, C. (2017). Assembling formation of highly dispersed Pd nanoparticles supported 1D carbon fiber electrospun with excellent catalytic active and recyclable performance for Suzuki reaction. *Applied Surface Science, 399*, 185–191.

Zare, K., Sadegh, H., Shahryari-Ghoshekandi, R., Maazinejad, B., Ali, V., Tyagi, I., Agarwal, S., & Gupta, V. K. (2015). Enhanced removal of toxic Congo red dye using multi walled carbon nanotubes: Kinetic, equilibrium studies and its comparison with other adsorbents. *Journal of Molecular Liquids, 212*, 266–271.

Zhang, M., Bacik, D. B., Roberts, C. B., & Zhao, D. (2013). Catalytic hydrodechlorination of trichloroethylene in water with supported CMC-stabilized palladium nanoparticles. *Water Research, 47*, 3706–3715. https://doi.org/10.1016/j.watres.2013.04.024

Zhang, Y., Zhao, Q., & Chen, B. (2022). Reduction and removal of Cr(VI) in water using biosynthesized palladium nanoparticles loaded *Shewanella oneidensis* MR-1. *Science of the Total Environment, 805*, 150336. https://doi.org/10.1016/j.scitotenv.2021.150336